Broadband couplers for hybrid silicon-chalcogenide glass photonic integrated circuits

Research Article | Vol. 27, No. 10 | 13 May 2019 | OPTICS EXPRESS 13781
Optics EXPRESS

Broadband couplers for hybrid silicon-chalcogenide glass photonic integrated circuits

Bin Shen,[1] Hongtao Lin,[2] Florian Merget,[1] Saeed Sharif Azadeh,[1] Chao Li,[3,6] Guo-Qiang Lo,[3,6] Kathleen A. Richardson,[4] Juejun Hu,[5] and Jeremy Witzens[1,*]

[1]*Institute of Integrated Photonics, RWTH Aachen University, Sommerfeldstr. 18/24, 52074 Aachen, Germany*
[2]*College of Information Science & Electronic Engineering, Zhejiang University, Hangzhou, China*
[3]*Institute of Microelectronics (IME)/ASTAR, Science Park Road 11, Singapore*
[4]*College of Optics and Photonics, University of Central Florida, 4304 Scorpius St., Orlando, FL 32816-2700, USA*
[5]*Department of Materials Science & Engineering, Massachusetts Institute of Technology, Cambridge, MA 02139, USA*
[6]*Currently with Advanced Micro Foundry Pte Ltd. (AMF), Singapore*
**jwitzens@iph.rwth-aachen.de*

Abstract: We report on the design, fabrication and testing of three types of coupling structures for hybrid chalcogenide glass $Ge_{23}Sb_7S_{70}$-Silicon (GeSbS-Si) photonic integrated circuit platforms. The first type is a fully etched GeSbS grating coupler defined directly in the GeSbS film. Coupling losses of 5.3 dB and waveguide-to-waveguide back-reflections of 3.4% were measured at a wavelength of 1553 nm. Hybrid GeSbS-to-Si butt couplers and adiabatic couplers transmitting light between GeSbS and Si single-mode waveguides were further developed. The hybrid butt couplers (HBCs) feature coupling losses of 2.7 dB and 9.2% back-reflection. The hybrid adiabatic couplers (HACs) exhibit coupling losses of 0.7 dB and negligible back-reflection. Both HBCs and HACs have passbands exceeding the 100 nm measurement range of the test setup. GeSbS grating couplers and GeSbS-to-Si waveguide couplers can be co-fabricated in the same process flow, providing, for example, a means to first couple high optical power levels required for nonlinear signal processing directly into GeSbS waveguides and to later transition into Si waveguides after attenuation of the pump. Moreover, GeSbS waveguides and HBC transitions have been fabricated on post-processed silicon photonics chips obtained from a commercially available foundry service, with a previously deposited 2 μm thick top waveguide cladding. This fabrication protocol demonstrates the compatibility of the developed integration scheme with standard silicon photonics technology with a complete back-end-of-line process.

1. Introduction

Silicon photonics (SiP) in the silicon-on-insulator (SOI) platform has attracted great interest in research and industry in the past decades [1]. Compatibility with the complementary metal oxide semiconductor (CMOS) technology has allowed for low-cost manufacturing and commercialization of SiP devices. Utilization of the free-carrier plasma dispersion effect, as well as integration with other selectively grown or heterogeneously integrated semiconductor materials has enabled a wide range of functionalities encompassing electro-optic modulation [2], photodetection [3] and light generation [4].

Si has a large refractive index and is transparent in the near infrared C- and O-communication bands. It also has a high optical damage threshold and high third order

#360673 https://doi.org/10.1364/OE.27.013781
Journal © 2019 Received 20 Feb 2019; revised 10 Apr 2019; accepted 11 Apr 2019; published 29 Apr 2019

nonlinearity, which are very important features for all optical signal processing and wavelength conversion [5]. However, these applications are limited by the large two-photon absorption (TPA) of Si [6]. One way to overcome this problem is to integrate chalcogenide glasses into the SOI platform. Chalcogenide glasses, which contain one or more of the chalcogen elements including S, Se and Te and are covalently formed with network formers such as Ge, Sb or As, have large third order nonlinearities and a much smaller TPA coefficient than that of Si [7]. Thanks to their remarkable optical properties such as large and tailorable refractive index, low loss, broad transparency region, and high optical nonlinearity, chalcogenide glasses have been demonstrated to be promising materials for a broad range of applications such as sensors [8,9], unconventional substrate integration [10,11], and all-optical signal processing [12]. Rekindled interest in nonlinear-based transmission by means of the nonlinear Fourier transform [13] may also increase interest in manipulation of solitons with highly nonlinear fibers [14,15] or on-chip waveguides [16]. In another optical communications application, phase sensitive amplification based on parametric amplification and its on-chip implementation has recently gained great interest [17]. Hybrid integration of As_2S_3 devices on silicon has enabled stimulated Brillouin scattering (SBS) [18], which allows bringing a number of applications such as SBS enabled tunable time delays [19] and SBS enabled ultrahigh-resolution spectroscopy [20] on chip [21].

While previous works have investigated hybrid waveguides composed of both chalcogenides and Si, for example by infiltration of a Si slot waveguide, thus also obtaining enhancement of the optical intensity inside the chalcogenide [22], here we completely transition between Si and GeSbS waveguides in order not to be penalized by Si TPA inside the GeSbS waveguides. One of the main issues of integrating chalcogenide glasses into the SOI platform in this way is to couple light to and from the chalcogenide devices. Here, we focus on the efficient coupling of light into GeSbS chalcogenide glass waveguides hybridly integrated into the SOI platform by post-processing of chips fabricated in a standard SiP foundry, Singapore's Institute of Microelectronics (IME). Another issue is to define a fabrication flow and device geometries that allow for post-processing of fully fabricated SiP chips with a fully fabricated back-end-of-line (BEOL) stack. Indeed, it is our objective to integrate GeSbS based devices in a fully functional *standard* SiP platform with electro-optic functionality. This prevents, for example, relying on additional etch-stop layers other than those already present in the process.

At a wavelength of 1550 nm, GeSbS has a refractive index of 2.17, a third order nonlinear index on the order of $10^{-18}\,\mathrm{m}^2/\mathrm{W}$, and negligible TPA [23,24]. It is important to note that reported values for these properties can vary widely depending on material form (bulk or planar film), measurement wavelength and specific characterization method. The linear loss of single-mode GeSbS waveguides can be as low as 0.5 dB/cm [25,26]. Compared to arsenic-based chalcogenide glasses, GeSbS has low toxicity.

In this paper, three types of coupling structures have been designed, fabricated and analyzed. First, we present the design and experimental validation of a fully etched GeSbS grating coupler (GC) allowing direct coupling of light into GeSbS waveguides (Section 2), which can be advantageous for the first signal processing stage, e.g. if optical power initially exceeds levels that can be transported in Si waveguides without incurring high TPA induced losses. Next, we demonstrate two couplers between GeSbS and silicon nanowire waveguides, a GeSbS-Si hybrid butt coupler (HBC), Section 3, and a GeSbS-Si hybrid adiabatic coupler (HAC), Section 4. These approaches are benchmarked against each other in terms of insertion losses and back-reflections.

In all three cases, GeSbS waveguides are fabricated out of a 500 nm thick film deposited on top of SiP chips after post-processing, enabling their co-fabrication in a common hybrid technology platform. Coupling structures provide connectivity to 900 nm wide, fully etched GeSbS waveguides, either directly from a standard single-mode optical fiber with a 10.4 μm mode field diameter (MFD) in the case of the GC, or to and from fully etched, 400 nm by 220

Optics EXPRESS

nm Si waveguides. The GeSbS waveguide geometry ensures single-mode operation as well as anomalous dispersion at 1550 nm. The latter allows efficient phase matching for parametric light generation, an important target application of chalcogenide materials. Inside test structures, GeSbS waveguide lengths (including tapered sections) are maintained as short as possible in order to minimize waveguide losses and are respectively 244 µm, 223 µm and 223 µm in the GC, HBC and HAC test structures. A GeSbS ring resonator (RR) coupled to the GeSbS bus waveguide is included in each of the test structures in order to independently monitor waveguide losses. All the GeSbS waveguides are air clad and located directly on top of the SOI wafer's buried oxide (BOX), or, in the case of the GCs, an oxidized Si wafer. Bending radii of 20 µm used in the GeSbS waveguide routing results in negligible excess losses – as verified by simulations – and do not skew the insertion losses extracted from experimental data.

2. GeSbS grating coupler

We first investigate fully etched GeSbS GCs for coupling of light to GeSbS single-mode waveguides. The fabrication process is facilitated by the joint fabrication of the fully etched GeSbS GCs and GeSbS waveguides in a single lithography and etch step. Here, light is directly injected into the GeSbS material, allowing a larger input optical power than if the light first transits through Si waveguides (as a consequence of the latter's large TPA). GeSbS-Si hybrid couplers described in the following sections allow transfer of light into the Si based devices after nonlinear processing.

2.1. GeSbS grating coupler design and fabrication

The focusing GC [27] is designed for coupling into a fiber mode with a forward coupling angle θ of 11 degrees [Fig. 1(a)] and a transverse electric (TE) polarization. The 500 nm thick chalcogenide layer is deposited on top of an oxidized Si wafer with a 3 µm thick SiO_2 layer using single-source thermal evaporation. After electron beam lithography (EBL) and reactive ion etching with CHF_3/CF_4 (3:1), the top of the GC is left air clad. Grooves as well as waveguides are fully etched. The full angle of the GC taper is 21 degrees, which is sufficient to let the beam freely diffract. Figure 1(b) shows an optical microscope image of a fabricated GC pair, connected by a waveguide loop coupled to a RR. The specific fabrication details can be found in [25].

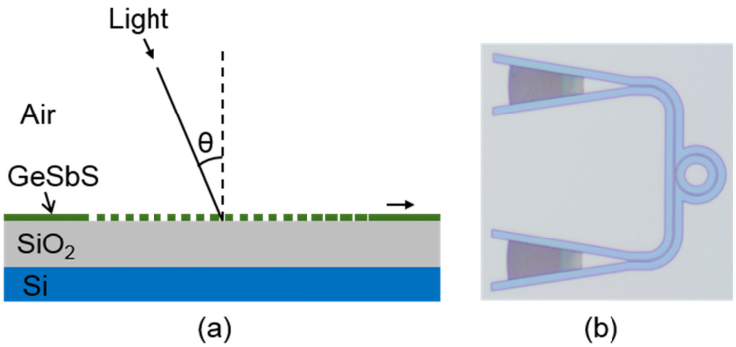

Fig. 1. (a) Schematic diagram of the GeSbS GC. (b) Optical microscope image of the fabricated GC pair, waveguide and ring resonator.

A grating period of 1341 nm with a trench width of 762 nm was first obtained with analytical calculations [28]. In order to further improve the coupling efficiency to an optical fiber mode with an MFD of 10.4 µm, the first 16 grooves were apodized [29]. The apodization starts with a trench width of 135 nm and a period of 1007 nm for the first trench located 34.9 µm from the end of the waveguide, and ends with the full 762 nm trench / 1341

Optics EXPRESS

nm period at the 17th trench. Apodization was iteratively optimized with finite-difference time-domain (FDTD) simulations performed with the commercial simulation tool RSOFT. Grating coupler insertion losses between single mode fiber and single mode GeSbS waveguide were simulated to be 4.9 dB at a wavelength of 1550 nm in a two-dimensional (2D) FDTD simulation.

2.2. GeSbS grating coupler insertion losses

Figure 2(a) shows the transmission spectrum of the fabricated GeSbS GC with an input power of 0 dBm. The radius of the RR is 100 μm, resulting in a free spectral range (FSR) of 1.54 nm. The minimum insertion loss of 10.6 dB is achieved at 1553 nm, which includes the loss resulting from two GCs and the 244 μm long waveguide. By fitting the resonance curve [Fig. 2(b)], we determine the intrinsic quality factor of the RR to be 110,000, corresponding to a waveguide loss of 4.0 dB/cm, wherein coupling losses and intrinsic waveguide losses could be distinguished from each other based on their wavelength dependence. While the coupling losses feature the expected increase with wavelength, the intrinsic losses remain in a tight range. Excess coupler losses were not deembedded so that the extracted waveguide losses might be overestimated. The loss from the short GeSbS waveguide is thus negligible, so that the loss per GC is extracted to be 5.3 dB. This coupler loss is better than the fully etched GeSbS GC loss of 7.5 dB reported by Serna et al. [30], and is slightly worse than that of shallow-etched GeSbS GCs reported by Chiles et al., 4.3 dB ± 0.7 dB [31]. However, comparing to the shallow-etched GCs, the fully etched GCs described here need fewer fabrication steps, making their fabrication much easier.

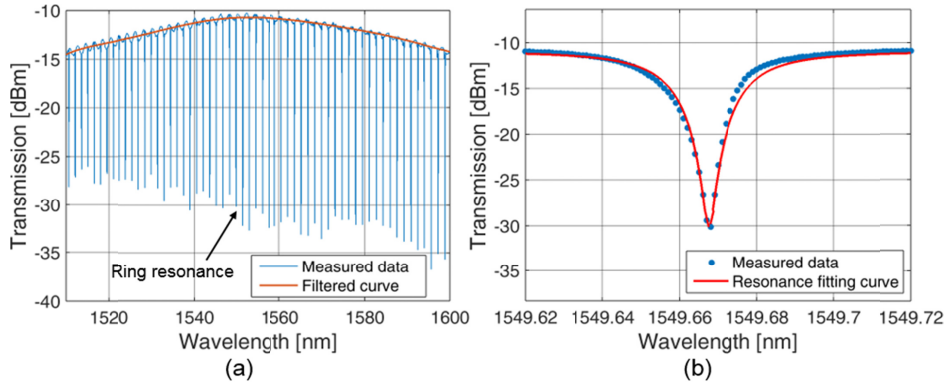

Fig. 2. (a) Transmission spectrum of the GeSbS device with an input power of 0 dBm. The smoothed transmission spectrum of the GC loop, with ripples filtered out, is shown by a red curve. (b) Measurement data (blue dots) in a smaller wavelength range around a resonance close to 1550 nm and its Lorentzian fit (red line).

As shown in Fig. 2(a), the 1 dB and 3 dB bandwidths of the GC pair are measured to be 39 nm and 80 nm, respectively. For a single GC, the 1 dB bandwidth is 60 nm, and the 3 dB bandwidth is limited by the wavelength range of the equipment. It is notable that the loss spectrum contains a 0.6 dB Fabry-Perot ripple, which is due to the back-reflection between the input and output GCs as corroborated by the FSR of 2.0 nm. By analyzing the Fabry-Perot resonance [32], we calculate that 3.4% of the light is back-reflected by each GC. Here and elsewhere in this paper smoothed transmission spectra [red curve in Fig. 2(a)] were obtained by applying a 1st order Savitzky-Golay smoothing filter after manually removing the resonances.

Optics EXPRESS

3. GeSbS-Si hybrid butt coupler

GeSbS-Si hybrid couplers are required to transmit light between GeSbS and Si single-mode waveguides. One intuitive hybrid coupler structure is the GeSbS-Si HBC, in which forward tapered GeSbS waveguides are butt-coupled to inverse tapered Si waveguides. This is similar to inverse couplers used for fiber-to-chip edge coupling [33] but further adapted to enable local BEOL removal. The goal here is to apply them to fully processed SiP chips.

3.1. GeSbS-Si hybrid butt coupler design and fabrication

In the HBC loop, light is coupled in and out of the chip through silicon GCs. The silicon GCs are followed by SiO_2 clad silicon waveguides with a thickness of 220 nm and a width of 400 nm, which are connected to a 500 nm thick GeSbS waveguide via the HBCs [Fig. 3(a)]. Figures 3(b) and 3(c) show a zoomed-in microscope image as well as a schematic of the HBC. To achieve maximum coupling efficiency, the coupling structure is designed so that the center of the Si waveguide mode lines up with the center of the GeSbS waveguide mode in both the vertical and horizontal directions. Therefore, the BEOL layer stack as well as 90 nm of the BOX layer are removed in the area of the GeSbS waveguide. To ensure a precise etch stop during BEOL removal, a partially etched Si device layer (deep-etched Si with a remaining slab height of 90 nm) is used as an etch stop. This Si layer is then removed during the same etch sequence by switching the etching chemistry. Finally, the top 90 nm of the BOX layer is removed by a third dry etch.

To avoid scattering at the onset of the etch stop layer, the silicon waveguide is adiabatically transformed from a fully etched ridge into a deep-etched rib waveguide. Over a length of 15 µm, the silicon waveguide slab is tapered up to a total width of 3 µm. At the same time, the silicon waveguide core is tapered down from 400 nm to 200 nm in order to expand the mode and match its dimensions to the GeSbS waveguide. The waveguide core (but not the 90 nm etch stop layer) is terminated 1 µm before the nominal GeSbS taper facet position to accommodate lithographic overlay tolerances. As a result of this process, a residual nominally 1 µm wide layer of deep-etched silicon remains between the end of the silicon rib waveguide and the facet of the GeSbS taper. A 40 µm long GeSbS taper adiabatically narrows the GeSbS waveguide from a parameterized initial width (see below) to the 900 nm standard single-mode waveguide width used in this work.

As shown in Fig. 3(a), all-silicon alignment loops (SAL) with SiO_2 cladding are fabricated on the chip besides the HBC loops. The SALs have the same silicon GCs as the HBC loops, which are connected with a 140 µm long silicon waveguide resulting in negligible additional losses. They are used as reference structures to obtain the silicon GC losses needed to deconvolve the HBC losses.

The silicon GCs and waveguides were fabricated within the IME SiP platform with 248 nm deep UV lithography [34]. The GeSbS HBC devices were fabricated by EBL and RIE during post-processing of the chips, with fabrication details in [25].

Optics EXPRESS

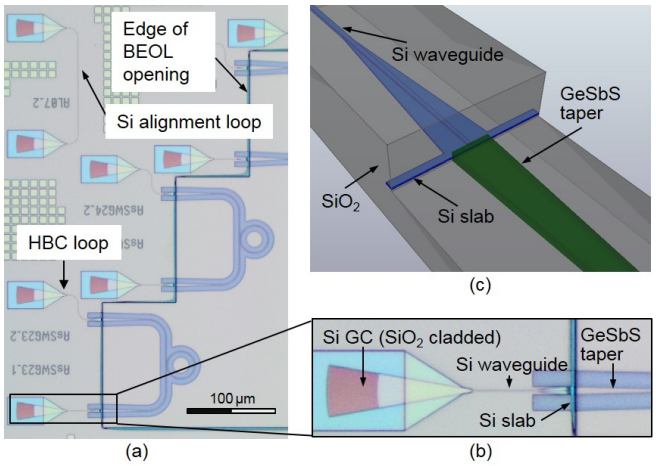

Fig. 3. (a) Optical microscope image of HBC loops and a Si reference loop. (b) Optical microscope image of a Si GC (SiO_2 clad) and a GeSbS-Si HBC. (c) Schematic view of a GeSbS-Si HBC.

3.2. GeSbS-Si hybrid butt coupling loss

Figure 4(a) shows the transmission spectra of an SAL and an HBC loop, both with an input power of 0 dBm. This HBC loop has a GeSbS taper width of 2.5 µm. The GeSbS waveguide loop is coupled to a RR with a radius of 15 µm, which results in an FSR of 9.9 nm. Since the minimum insertion loss of both loops is obtained at 1552 nm, we use it as the reference wavelength for the loss comparison (since it is also the wavelength at which data analysis is the most robust against GC peak wavelength variations). The total insertion losses of the SAL and HBC loops are respectively 6.8 dB and 12.2 dB at 1552 nm.

By fitting the resonance of the GeSbS RR, we extract losses of 5.5 dB/cm. Therefore, the optical loss resulting from the 223 µm long GeSbS waveguide loop is also negligible. Thus, by subtracting the insertion loss of the SAL from the insertion loss of the HBC loop, we get the HBC loss

$$Hybrid\ Coupler\ Loss = \frac{Insertion\ Loss\ (HBC\ Loop) - Insertion\ Loss\ (SAL)}{2} \quad (1)$$

Figure 4(b) shows the loss spectrum of the HBC, with 2.7 dB losses at 1552 nm. The 1 dB and 3 dB optical bandwidths of the SAL and HBC loops are both 28 nm and 49 nm, respectively. Thus, the optical bandwidth of the HBC loop is determined by the silicon GCs. We can see in Fig. 4(b) that the 1 dB bandwidth of a single HBC is larger than 100 nm, which is the measurement range limit of our equipment.

The loss spectrum of the HBC contains 1.6 dB Fabry-Perot ripples, which is attributed to the back-reflection between the GeSbS-Si coupling facets as also corroborated by an FSR of 2.1 nm correlating with the 223 µm GeSbS waveguide length [note that Fig. 4(b) shows half the ripple strength since the transfer function of the loop, in dB, has been halved to normalize the losses to a single GC]. By analyzing the Fabry-Perot resonances [32], we evaluate the HBC reflection to be 9.2%.

A series of HBC loops with varying taper width have been fabricated to characterize its influence on the HBC loss. Figure 5 shows the simulated and measured HBC losses at 1552 nm as a function of the GeSbS taper width. In the measured data, the HBC has a minimum loss of 2.7 dB with a GeSbS taper width of 2.5 µm. Overall, good agreement is found between simulated and measured HBC losses; in particular, dependency on GeSbS taper width is predicted well.

Optics EXPRESS

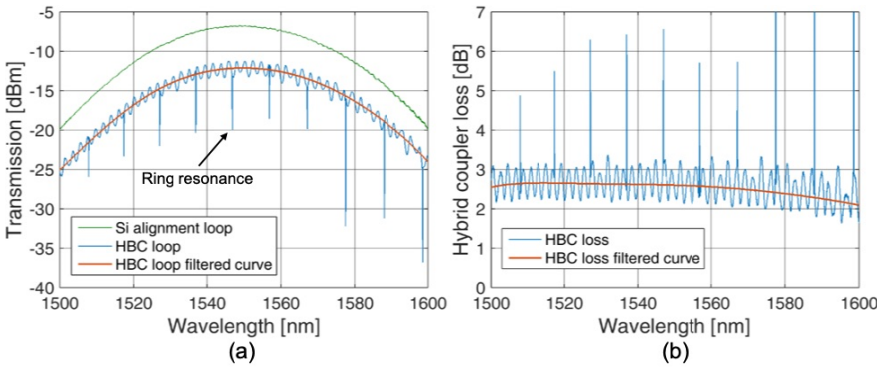

Fig. 4. (a) Transmission spectra of SAL (green line) and HBC loops (blue line) with an input power of 0 dBm. The smoothed transmission spectrum of the HBC loop, with ripples filtered out, is shown by a red curve. (b) Raw HBC loss spectrum featuring ripples (blue line) and its filtered version (red line).

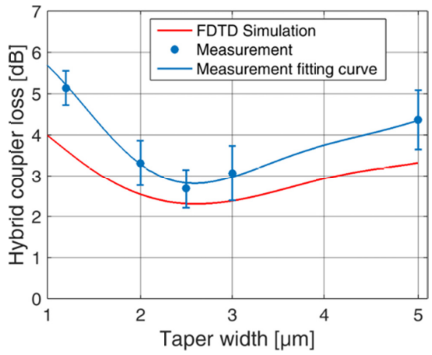

Fig. 5. Simulated (red line), measured (blue dots) and interpolated (blue line) HBC losses as a function of GeSbS taper width. The error bars correspond to the magnitude of the Fabry-Perot ripples. The blue curve is a polynomial fit to help guiding the eye.

4. GeSbS-Si hybrid adiabatic coupler

In order to minimize hybrid coupling loss as well as back-reflections at the interface, we have designed and fabricated HAC type couplers. These have a similar principle of operation as SiP edge couplers consisting in mode size converters with an inverse tapered silicon waveguide embedded in a larger core waveguide made out of lower refractive index materials such as polymers or SiON [35]. Morrison et al. have demonstrated As_2S_3 HAC to transmit light between single-mode Si waveguides and As_2S_3 waveguides for SBS with low hybrid coupling loss [18]. Here, we adapt these couplers to the Si-GeSbS material system with film thicknesses compatible with prior grating coupling of the light. This allows in particular to show the possibility of co-fabricating them with GCs, as well as to compare their performance with the previously described HBCs. Since, as described below, the HBCs are easier to fabricate in standard SiP chips by means of BEOL deprocessing, a comparison of performance will help to trade-off fabrication complexity with performance.

4.1. GeSbS-Si hybrid adiabatic coupler design and fabrication

In the HAC loops, light is coupled in and out of the chip through silicon GCs [Fig. 6(a)]. The standard 400 nm (width) by 220 nm (height) waveguides are tapered down to a width of 200 nm (compatible with the 248 nm DUV lithography) over a taper length of 15 μm. Here, both the silicon GCs and the silicon waveguides are air clad, as the SiP photonic integrated circuit (PIC) was taken from the fabrication facility before back-end fabrication. Figures 6(b) and

Optics EXPRESS

6(c) show a magnified microscope image as well as a schematic view of an HAC. A 500 nm GeSbS film is deposited on top of the chip and subsequently etched to form GeSbS waveguides. A GeSbS waveguide with a parameterized initial width overlays the entire Si taper. After termination of the Si taper, the GeSbS waveguide is tapered down to the standard 900 nm width over a length of 40 µm. Figure 6(d) shows a scanning electron microscope (SEM) image of the GeSbS-Si overlay. It can be seen that the GeSbS film forms a bump where it overlays the Si waveguide. The cross section of the GeSbS bump is close to an isosceles trapezoid with upper and lower widths of respectively 400 nm and 608 nm. Since the SEM image was taken at an angle, the height of the bump cannot be directly extracted from the micrograph. However, based on rescaling of the known 500 nm height of the GeSbS film, the height of the bump was verified to be approximately 220 nm, coinciding as expected with the Si waveguide height. Figure 6(e) shows the cross section of the coupler at the point where the overlay starts, as assumed in the 3D-FDTD simulation. As the Si waveguide is tapered down along the main axis of the coupler, the GeSbS bump is also tapered down by the same amount, with a constant offset maintained between the waveguide width and the lower width of the isosceles trapezoid. The differences between the simulated HAC coupler losses with and without the GeSbS bump are negligible.

As shown in Fig. 6(a), a pure silicon alignment loop with air cladding (SAL_{air}) is fabricated on the chip besides the HAC loops. The SAL_{air} comprises the same Si GC as in the previous section, as well as a 140 µm long silicon waveguide. However, insertion losses and peak wavelength are changed due to the top air cladding.

Here too, the Si PICs were fabricated within the IME SiP platform with 248 nm deep UV lithography [34] and subsequently post-processed with EBL after GeSbS film deposition.

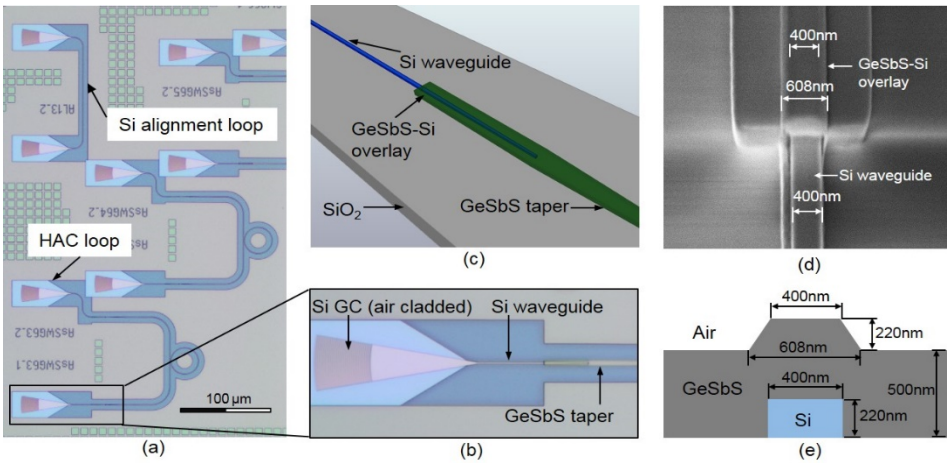

Fig. 6. (a) Optical microscope image of HAC loops and a Si reference loop. (b) Optical microscope image of a Si GC (air clad) and a GeSbS-Si HAC. (c) Schematic view of a GeSbS-Si HAC. (d) SEM image of the front facet of the GeSbS-Si overlay. (e) Cross-section of the starting point of the GeSbS-Si overlay in the FDTD simulations.

4.2. GeSbS-Si hybrid adiabatic coupling loss

Figure 7(a) shows the transmission spectra of a SAL_{air} and a HAC loop with an input power of 0 dBm. This HAC loop has an initial GeSbS taper width of 1.5 µm. As for the HBC loops, the GeSbS waveguide of the HAC loops is coupled to a 15 µm RR with an FSR of 9.9 nm. The minimum loss of the SAL_{air} is obtained at 1523 nm, at which the insertion losses of the SAL_{air} and of the HAC loop are respectively 9.1 dB and 10.5 dB. By fitting the resonance of the GeSbS RR, we extract losses of 5.6 dB/cm. Similarly to the HBC chip, the waveguide losses inside the SAL_{air} and HAC loop are negligible. The HAC loss is half of the insertion

Optics EXPRESS

losses of the HAC loop after subtraction of the SAL_{air} losses. At 1523 nm, the HAC features 0.7 dB insertion loss.

The 1 dB bandwidth of the SAL_{air} and of the HAC loop are 37 nm and 38 nm, respectively. The 3 dB bandwidth of the SAL_{air} and of the HAC loop are larger than 54 nm and 57 nm, respectively, with the measured 3 dB bandwidth of the HAC loop limited by the wavelength range of the equipment. Figure 7(b) shows the extracted loss spectrum of the HAC. As for the HBC, the deembedded 1 dB bandwidth of the HAC is larger than 100 nm, the measurement range limit of our equipment.

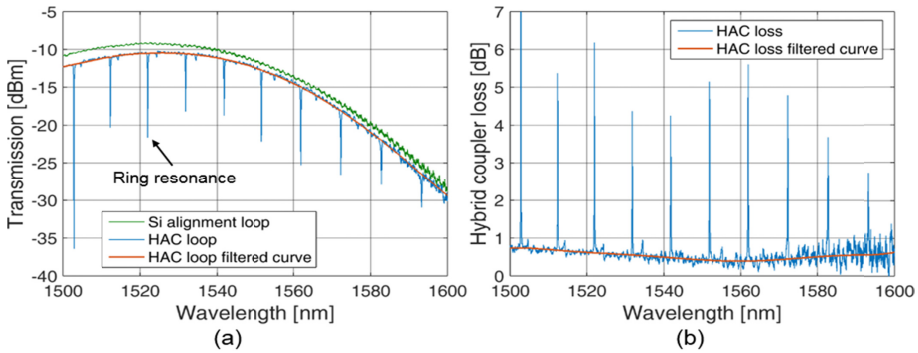

Fig. 7. (a) Transmission spectra of an SAL_{air} (green line) and HAC loop (blue line) with an input power of 0 dBm. The smoothed transmission spectrum of the HAC loop is shown as a red curve. (b) HAC loss spectrum (blue line) and its smoothed equivalent (red line).

The loss spectrum of the HAC loop does not contain any obvious Fabry-Perot ripples (small ripples due to the Si GCs are present in the raw spectra of both loops and cancel out), which means that the HAC loop does not induce obvious back-reflection as seen in the HBC loop.

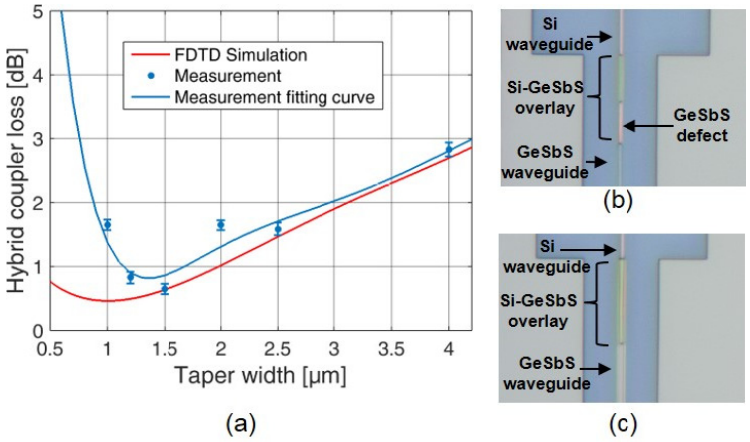

Fig. 8. (a) Simulated (red line), measured (blue dots) and interpolated (blue line) HAC losses as a function of GeSbS taper width. The error bars correspond to the standard deviations of the measured losses. Optical microscope images of the GeSbS-Si HACs with initial GeSbS taper widths of 0.5 µm (b) and 1.5 µm (c). As in Fig. 5, the blue curve is a polynomial fit to help guiding the eye.

A series of HAC loops with variations of the initial taper width have been fabricated to characterize its influence on HAC loss. Figure 8(a) shows the simulated and measured HAC losses at 1523 nm as a function of the GeSbS taper width. The HAC loss with GeSbS taper width of 0.5 µm is 10.6 dB, and was omitted from the figure in order to keep the y-axis in a narrower range. The minimum measured HAC loss is 0.7 dB at a GeSbS taper width of 1.5

Optics EXPRESS

µm. Good agreement is observed between simulated and measured losses for taper widths larger than 1.2 µm. However, for smaller GeSbS taper widths, measured losses become significantly larger than simulated losses. After visual inspection of the chips in an optical microscope, it appears this is caused by the GeSbS waveguide having defects in the region overlaying the Si waveguide for small GeSbS taper widths; such defects were not found for the wider tapers. Figures 8(b) and 8(c) show microscope images of GeSbS-Si HACs with GeSbS taper widths of 0.5 µm and 1.5 µm, respectively. We can see that in the GeSbS-Si overlay region, the HAC with 0.5 µm taper width is missing a piece of GeSbS waveguide, while the HAC with the 1.5 µm taper is free of defects.

Since the HAC couplers appear the superior devices in terms of back-reflection and insertion losses, it would be desirable to also implement them with a device configuration and a process flow compatible with fully fabricated SiP chips including a full BEOL process, as available from commercial foundry platforms. This would, however, be considerably harder for the HACs than for the previously described HBCs. While one could also envision replacing the fully etched ridge waveguides used in the HACs by partially etched rib waveguides in order to provide an etch stop at the bottom of the BEOL stack, this would only partially resolve the problem due to the resulting topology of the etch stop layer (since for the HACs the Si waveguide has to extend into the region where the BEOL is deprocessed). Wet SiO_2 etches can be highly selective to a Si etch stop layer, however they cause their own set of difficulties, such as undercutting of the protected areas. Dry etches typically used to etch SiO_2 based on CHF_3 or fluorocarbons (C_xF_y), while providing some selectivity [36], also attack Si, so that the Si waveguiding layer appears likely to be damaged in such a process in the absence of other non-standard etch stop layers not available in standard SiP chips. The Si etch stop layer used for HBC fabrication on the other hand does not serve for waveguiding, is planar, and is completely removed as part of subsequent etches. Consequently, etch selectivity is much less of an issue there and the optical quality of resulting structures thus not as severally impacted.

The overall resilience of the utilized GeSbS material across the range of process conditions applied in this paper is also noteworthy, in particular its ability to maintain its optical properties and to remain relatively free of defects. This is all the more remarkable since other chalcogenide materials such as As_2S_3 or As_2Se_3 have historically suffered from large variability in their post-deposition properties as well as increased defectivity.

5. Conclusions

Three types of coupling structures to GeSbS waveguides compatible with hybrid integration in a silicon photonics platform have been shown. The fully etched GeSbS grating coupler has a loss of 5.3 dB and results in 3.4% of the light being back-reflected into the GeSbS waveguide when it is coming from the latter. This grating coupler also allows injecting light directly into GeSbS, without a first Si based waveguide segment limiting the power, when nonlinear processing is targeted in a first device stage. Two alternatives, hybrid butt couplers and hybrid adiabatic couplers have been applied to transition between GeSbS and Si single-mode waveguides. The HBC has a 2.7 dB loss and 9.2% of the light is back reflected when injected from the GeSbS waveguide. The HAC has a reduced loss of 0.7 dB and negligible back-reflection.

While the HAC has better performance, both in terms of insertion losses and back-reflection, we were able to fabricate the HBCs on standard chips on which the back-end-of-line stack had been locally deprocessed. The HACs on the other hand were fabricated on chips from a wafer without back-end-of-line stack. In view of combining chalcogenide waveguides with a fully functional silicon photonics platform, the ability to easily deprocess the back-end-of-line is a big advantage. All devices have been designed and fabricated with the same GeSbS film thickness, so that the GeSbS-to-Si waveguide transitions can be co-fabricated with the grating couplers. For example, initial light injection into GeSbS

Optics EXPRESS

waveguides via grating couplers can be combined with a downstream transition into Si waveguides. Compatibility of waveguide transition geometries with back-end-of-line deprocessing is expected to be instrumental to combine GeSbS waveguides with the entire set of functionalities already available in standard silicon photonics platforms.

Funding

Deutsche Forschungsgemeinschaft (DFG) (403153975).

References

1. R. Soref, "The past, present, and future of silicon photonics," J. Sel. Top. Quant. Electron. **12**(6), 1678–1687 (2006).
2. J. Witzens, "High-speed silicon photonics modulators," Proc. IEEE **106**(12), 2158–2182 (2018).
3. L. Vivien, J. Osmond, J.-M. Fédéli, D. Marris-Morini, P. Crozat, J.-F. Damlencourt, E. Cassan, Y. Lecunff, and S. Laval, "42 GHz p.i.n Germanium photodetector integrated in a silicon-on-insulator waveguide," Opt. Express **17**(8), 6252–6257 (2009).
4. G. H. Duan, C. Jany, A. Le Liepve, A. Accard, M. Lamponi, D. Make, P. Kaspar, G. Levaufre, N. Girard, F. Lelarge, J.-M. Fedeli, A. Descos, B. Ben Bakir, S. Messaoudene, D. Bordel, S. Menezo, G. de Valicourt, S. Keyvaninia, G. Roelkens, D. Van Thourhout, D. J. Thompson, F. Y. Gardes, and G. T. Reed, "Hybrid III-V on silicon lasers for photonic integrated circuits on silicon," J. Sel. Top. Quant. Electron. **20**(4), 6100213 (2014).
5. B. Jalali and S. Fathpour, "Silicon photonics," J. Lightwave Technol. **24**(12), 4600–4615 (2006).
6. G. Priem, P. Bienstman, G. Morthier, and R. Baets, "Impact of absorption mechanisms on Kerr-nonlinear resonator behavior," J. Appl. Phys. **99**(6), 63103 (2006).
7. B. J. Eggleton, B. Luther-Davies, and K. Richardson, "Chalcogenide photonics," Nat. Photonics **5**(3), 141–148 (2011).
8. M.-L. Anne, J. Keirsse, V. Nazabal, K. Hyodo, S. Inoue, C. Boussard-Pledel, H. Lhermite, J. Charrier, K. Yanakata, O. Loreal, J. Le Person, F. Colas, C. Compère, and B. Bureau, "Chalcogenide glass optical waveguides for infrared biosensing," Sensors (Basel) **9**(9), 7398–7411 (2009).
9. D. M. Kita, H. Lin, A. Agarwal, K. Richardson, I. Luzinov, T. Gu, and J. Hu, "On-chip infrared spectroscopic sensing: redefining the benefits of scaling," J. Sel. Top. Quant. Electron. **23**(2), 340–349 (2017).
10. L. Li, H. Lin, S. Qiao, Y. Zou, S. Danto, K. Richardson, J. D. Musgraves, N. Lu, and J. Hu, "Integrated flexible chalcogenide glass photonic devices," Nat. Photonics **8**(8), 643–649 (2014).
11. H. Lin, Y. Song, Y. Huang, D. Kita, S. Deckoff-Jones, K. Wang, L. Li, J. Li, H. Zheng, Z. Luo, H. Wang, S. Novak, A. Yadav, C.-C. Huang, R.-J. Shiue, D. Englund, T. Gu, D. Hewak, K. Richardson, J. Kong, and J. Hu, "Chalcogenide glass-on-graphene photonics," Nat. Photonics **11**(12), 798–805 (2017).
12. V. G. Ta'eed, M. Shokooh-Saremi, L. Fu, D. J. Moss, M. Rochette, I. C. M. Littler, B. J. Eggleton, Y. Ruan, and B. Luther-Davies, "Integrated all-optical pulse regenerator in chalcogenide waveguides," Opt. Lett. **30**(21), 2900–2902 (2005).
13. S. K. Turitsyn, J. E. Prilepsky, S. T. Le, S. Wahls, L. L. Frumin, M. Kamalian, and S. A. Derevyanko, "Nonlinear Fourier transform for optical data processing and transmission: advances and perspectives," Optica **4**(3), 307–322 (2017).
14. L. Melnikov, "Soliton fission and fusion in dispersion oscillating fiber and correlation properties of the pulses," in *International Conference Laser Optics* (IEEE, 2016) pp. R8–7.
15. S. Li, J. Koch, and S. Pachnicke, "Optical signal processing in the discrete nonlinear frequency domain," in *Optical Fiber Communication Conference* (Optical Society of America, 2018), paper W2A.40.
16. X. Gai, S. Madden, D.-Y. Choi, D. Bulla, and B. Luther-Davies, "Dispersion engineered $Ge_{11.5}As_{24}Se_{64.5}$ nanowires with a nonlinear parameter of 136 $W^{-1}m^{-1}$ at 1550 nm," Opt. Express **18**(18), 18866–18874 (2010).
17. E. Liebig, I. Sackey, T. Richter, A. Gajda, A. Peczek, L. Zimmermann, K. Petermann, and C. Schubert, "Performance evaluation of a silicon waveguide for phase regeneration of a QPSK signal," J. Lightwave Technol. **35**(6), 1149–1156 (2017).
18. B. Morrison, A. Casas-Bedoya, G. Ren, K. Vu, Y. Liu, A. Zarifi, T. G. Nguyen, D.-Y. Choi, D. Marpaung, S. J. Madden, A. Mitchell, and B. J. Eggleton, "Compact Brillouin devices through hybrid integration on silicon," Optica **4**(8), 847–854 (2017).
19. T. Schneider, M. Junker, and K.-U. Lauterbach, "Time delay enhancement in stimulated-Brillouin-scattering-based slow-light systems," Opt. Lett. **32**(3), 220–222 (2007).
20. S. Preußler, A. Wiatrek, K. Jamshidi, and T. Schneider, "Ultrahigh-resolution spectroscopy based on the bandwidth reduction of stimulated Brillouin scattering," IEEE Photonics Technol. Lett. **23**(16), 1118–1120 (2011).
21. B. J. Eggleton, C. G. Poulton, and R. Pant, "Inducing and harnessing stimulated Brillouin scattering in photonic integrated circuits," Adv. Opt. Photonics **5**(4), 536–587 (2013).
22. P. W. Nolte, C. Bohley, and J. Schilling, "Tuning of zero group velocity dispersion in infiltrated vertical silicon slot waveguides," Opt. Express **21**(2), 1741–1750 (2013).

Optics EXPRESS

23. J. W. Choi, Z. Han, B.-U. Sohn, G. F. R. Chen, C. Smith, L. C. Kimerling, K. A. Richardson, A. M. Agarwal, and D. T. H. Tan, "Nonlinear characterization of GeSbS chalcogenide glass waveguides," Sci. Rep. **6**(1), 39234 (2016).
24. S. Serna, H. Lin, C. Alonso-Ramos, A. Yadav, X. Le Roux, K. Richardson, E. Cassan, N. Dubreuil, J. Hu, and L. Vivien, "Nonlinear optical properties of integrated GeSbS chalcogenide waveguides," Photon. Res. **6**(5), B37–B42 (2018).
25. Q. Du, Y. Huang, J. Li, D. Kita, J. Michon, H. Lin, L. Li, S. Novak, K. Richardson, W. Zhang, and J. Hu, "Low-loss photonic device in Ge-Sb-S chalcogenide glass," Opt. Lett. **41**(13), 3090–3093 (2016).
26. J.-É. Tremblay, M. Malinowski, K. A. Richardson, S. Fathpour, and M. C. Wu, "Picojoule-level octave-spanning supercontinuum generation in chalcogenide waveguides," Opt. Express **26**(16), 21358–21363 (2018).
27. R. Waldhäusl, B. Schnabel, P. Dannberg, E.-B. Kley, A. Bräuer, and W. Karthe, "Efficient coupling into polymer waveguides by gratings," Appl. Opt. **36**(36), 9383–9390 (1997).
28. L. Chrostowski and M. Hochberg, *Silicon Photonics Design* (Cambridge University, 2015).
29. D. Taillaert, P. Bienstman, and R. Baets, "Compact efficient broadband grating coupler for silicon-on-insulator waveguides," Opt. Lett. **29**(23), 2749–2751 (2004).
30. S. Serna, H. Lin, C. Alonso-Ramos, A. Yadav, X. Le Roux, K. Richardson, E. Cassan, N. Dubreuil, J. Hu, and L. Vivien, "Linear and third order nonlinear optical properties of GeSbS chalcogenide integrated waveguides," in *14th International Conference on Group IV Photonics* (IEEE, 2017), pp. 109–110.
31. J. Chiles, M. Malinowski, A. Rao, S. Novak, K. Richardson, and S. Fathpour, "Low-loss, submicron chalcogenide integrated photonics with chlorine plasma etching," Appl. Phys. Lett. **106**(11), 111110 (2015).
32. N. Ismail, C. C. Kores, D. Geskus, and M. Pollnau, "Fabry-Pérot resonator: spectral line shapes, generic and related Airy distributions, linewidths, finesses, and performance at low or frequency-dependent reflectivity," Opt. Express **24**(15), 16366–16389 (2016).
33. J. Cardenas, C. B. Poitras, K. Luke, L.-W. Luo, P. A. Morton, and M. Lipson, "High coupling efficiency etched facet tapers in silicon waveguides," IEEE Photonics Technol. Lett. **26**(23), 2380–2382 (2014).
34. Advanced Micro Foundry Pte Ltd, *http://www.advmf.com*.
35. T. Tsuchizawa, K. Yamada, H. Fukuda, T. Watanabe, J.-I. Takahashi, M. Takahashi, T. Shoji, E. Tamechika, S. Itabashi, and H. Morita, "Microphotonics devices based on silicon microfabrication technology," J. Sel. Top. Quant. Electron. **11**(1), 232–240 (2005).
36. F. Gaboriau, G. Carthy, M.-C. Peignon, and C. Cardinaud, "Selective and deep plasma etching of SiO_2: comparison between different fluorocarbon gases (CF_4, C_2F_6, CHF_3) mixed with CH_4 or H_2 and influence of the residence time," J. Vac. Sci. Technol. B **20**, 1514–1521 (2002).